Crystal growth and melting in NiZr alloy: Linking phase-field modeling to molecular dynamics simulations

M. Guerdane,[1] F. Wendler,[1] D. Danilov,[1,*] H. Teichler,[2] and B. Nestler[1]
[1]*Institute of Materials and Processes, Karlsruhe University of Applied Sciences, 76133 Karlsruhe, Germany*
[2]*Institute for Materials Physics, University of Göttingen, 37077 Göttingen, Germany*
(Received 9 December 2009; revised manuscript received 25 May 2010; published 16 June 2010)

We compare results from molecular dynamics simulations with those from phase-field modeling concerning the solidification and melting kinetics of a planar $[Ni_cZr_{1-c}]_{liquid}$-$Zr_{crystal}$ interface. Our study is an illustration that both approaches may predict the same quantitative physical description when the key parameters calculated within the atomistic molecular dynamics approach are used to construct the mesoscopic phase-field model. We show in this way that a thermodynamic consistent phase-field model can be applied down to the range of atomic structure. At the same time, molecular dynamics simulation seems to be capable to treat correctly relaxation dynamics, driven by thermodynamic forces, in a nonequilibrium state of solidification and melting. We discuss, in particular, how the free energy from atomistic calculations is used to design the phase dependent free-energy density in the phase-field model. Bridging the gap between both simulation approaches contributes to a better understanding of the thermodynamic and kinetic processes underlying the solidification and melting processes in alloys out of chemical equilibrium. The effective thermodynamic enhancement of the diffusivity through the strong negative enthalpy of mixing in the NiZr solution is discussed.

DOI: 10.1103/PhysRevB.81.224108 PACS number(s): 64.60.De, 64.70.D−, 65.20.De

I. INTRODUCTION

The need for multiscale modeling is motivated by the fact that important phenomena in materials sciences often involve interactions between microscopic and macroscopic length and time scales.[1,2] Considering the solidification process, for instance, solid-liquid interfaces are on the order of a few angstroms, whereas microstructural features are on the length of tens of micrometers. Time scales of solidification span from picoseconds for the typical atomic dynamics processes, taking place at the interface, to seconds needed for transport of heat and matter away from the interface. Understanding the physics of solidification over such disparate length and time scales, about ten orders of magnitude, represents one of the challenges of present materials sciences, for which new mathematical models and numerical simulations algorithms have to be developed. The central challenge quantitative multiscale models face is to ensure that descriptions at all scale levels are consistent with each other. The need for consistency requires a coupling between the microscopic and macroscopic descriptions. This can be achieved through transferring microscopic (atomic) key parameters into the macroscopic continuum models or, in cases of a strong coupling between fine and larger scales, by concurrently modeling at both scales.[3]

Here we are specifically interested in the question of whether and how molecular dynamics (MD) modeling, which is an atomistic description of matter, can be used to calibrate a phase-field (PF) model, which is in turn a mesoscopic and macroscopic approach in materials sciences. MD-based methods have recently been used for a broad range of applications to determine key thermophysical parameters of PF models.[4,5] A special need is for those parameters that are not easily accessible to experiments such as the magnitude of the interface energy, the kinetic coefficient and their anisotropy, as well as the component-resolved atom diffusivity in the melt. Both approaches, MD and PF, have their conventional length scales of optimal applicability. Transferring parameters from one method to the other raises the question of the equivalence of both treatments. Testing the equivalence needs detailed comparison of the predictions of the considered approaches for appropriate situations. This test is of particular importance, as it will prove the range of applicability of the treatments and will make obvious whether the two methods describe well the same aspects of physics, regardless of their inevitably different assumptions and approximations.

In the present work, we carry out such a quantitative test by confronting results from MD simulations with predictions of PF modeling in the case of the propagation of a planar $[Ni_cZr_{1-c}]_{liquid}$-$Zr_{crystal}$ interface during solidification and melting. An equilibrated crystal-liquid system at temperature T is set up away from chemical equilibrium by subjecting it to an abrupt temperature change ΔT that could be negative or positive. The sign of ΔT corresponds in our case to an undersaturated or supersaturated solution, respectively. The system will then evolve in the direction of the equilibrium state by growing or dissolving of the crystalline part. The propagation dynamics of the crystal-melt interface is then considered and the evolution in time of the concentration profiles is investigated as the system relaxes toward the equilibrium concentration described by the liquidus line of the phase diagram.

In a recent work,[6] we carried out a first attempt to link MD modeling to PF method regarding the $[Ni_cZr_{1-c}]_{liquid}$-$Zr_{crystal}$ interface dynamics. Considering the concentration profile and the propagation velocity of the crystal-liquid interface, we found that one had to increase the diffusion coefficients in the PF model by a factor 4 against their MD estimates in order to get acceptable agreement between both modeling methods. Those findings led us to the conclusion that bridging the gap between MD and PF model

treatments cannot be achieved by simply exchanging parameters but effects related to the inevitably different assumptions of both approaches have to be carefully considered. The question of the role of the activity coefficient in the chemical potential has been especially posed. We raised the doubt whether in the PF model an ideal solution form of the free energy (FE) for the melt reasonably captures the thermodynamic effects (e.g., the gradient of the chemical potential) in the vicinity of the crystal-liquid interface. The FE density for the crystal and liquid has been designed to reproduce the MD-calculated phase diagram.

Here we go a step further by using the FE density in the PF model as calculated in earlier work[7,8] for NiZr alloy by means of MD simulations. Computational evaluation of the entropy and FE of liquids, and disordered systems in general, has been a challenging task to atomistic simulations since long because it deserves elaborated treatments to take care of the statistical aspects of these key quantities. At present, PF modeling uses at best FE data from CALPHAD analysis—or related methods—of experimental parameters or they rely on phenomenological models to construct the FE density of a given system. All these methods are based on approximation models of the interatomic interactions, mostly the regular solution model. In this sense, MD modeling acquires a particular importance because it opens new possibilities for calculating the FE and entropy of the liquid phase. The FE calculated for NiZr alloy, within the MD model used here, leads to a phase diagram[7] which is in good agreement with the experimental one. This and other features (see Sec. II A) show that the considered MD model is able to describe in a reasonable way the thermodynamic equilibrium properties of the NiZr system. Originally, the present MD model was designed and extensively used in analyzing relaxation dynamics and glass forming properties of NiZr melts.[9] By dealing here with solidification and melting simulations, we address implicitly the question whether isothermal nonequilibrium MD simulations are able to treat properly relaxation dynamics driven by thermodynamic forces. We expect to answer this question by linking MD simulations to PF modeling, as the latter is a thermodynamic model designed to describe mainly nonequilibrium situations. At the same time, we address the question whether a thermodynamic consistent PF model is applicable down to the range of atomic structure, without thermodynamic concepts loosing their relevance at the atomic level.

Over the last decade, the PF method has emerged as a powerful computational approach to model solidification processes and microstructure formation, such as dendritic evolution and cellular growth, on mesoscopic and macroscopic scales.[10,11] The problem of sharp boundaries is circumvented by making the phase boundaries spatially diffuse over some width ε with the help of a scalar field ϕ that distinguishes between different phases. The evolution equations, which connect phase and diffusion fields, can be derived in a thermodynamically consistent way by demanding that the entropy increases locally for the system. The parameters which appear in the evolution equations cannot be derived within the framework of the phenomenological PF model. Therefore, they have to be imported from other considerations of those processes, i.e., by direct experimental measurements or by simulations based on other modeling methods. Due to the difficulty inherent in performing direct experimental measurements of solid-liquid interface properties, atomistic computer simulations have become more and more an important tool in providing necessary information about the factors which control thermodynamic and kinetic properties of the interfaces. Quantitative multiscale PF modeling of dendritic solidification in undercooled Ni melts, for instance, became possible[5] after MD simulations had provided the anisotropy of capillary and kinetic properties (that is, the interface tension σ and kinetic coefficient μ, respectively).[12] The shape and growth velocity of the dendrites depend sensitively on the degree of these anisotropies which can accurately be evaluated by different MD-based methods, whereas measuring them experimentally remains a difficult task.

There are only few atomistic simulation works in the literature on the kinetic processes of crystallization in alloys.[12–15] Particularly the atomic processes taking place at the crystal-liquid interface remain poorly understood. This may explain why until today an adequate model still is lacking, which properly describes the kinetic processes on the atomic scale during crystallization and melting. The classical model of Wilson and Frenkel[16,17] and its modified version of Broughton *et al.*[18] have successfully been applied for many pure materials[19,20] but fail to describe crystallization behavior in alloys.[21] In an atomistic MD study of a Lennard-Jones binary system, Celestini and Debierre[15] used a forced interface velocity technique to investigate the solute trapping effect. Their simulation results validate existing growth models regarding the relation between the segregation coefficient and the interface velocity. Recently, Kerrach *et al.*[21] carried out an MD study on the melting and crystallization of a more realistic alloy model, the intermetallic compound $Al_{50}Ni_{50}$, using embedded-atom potentials for the interatomic interactions. The significant discrepancy between their results and the classical growth model of Wilson and Frenkel, which in this case overestimates the growth velocity, is traced back to a neglection of the diffusion in the crystal-liquid interface by the latter model. They suggest that this often neglected effect has to be taken into account by theories aimed at describing the crystal growth on a quantitative level. Celestini and Debierre[15] came to the same conclusion in the above cited work.

A recent promising research direction is the development of phase-field crystal (PFC) models.[22] This approach allows performing simulations over time scales relevant for mesoscopic structure evolution by incorporating naturally the structure of the atomic density of the material. Another advantage of the PFC approach in comparison with the conventional PF modeling is its ability to predict some of the key physical parameters such as interfacial energies and their related anisotropies.[23] In a very recent work, Chan *et al.*[24] showed that PFC can be extended to describe not only the collective behavior but also the motions of individual atoms. The resulting extended approach is equivalent to MD modeling on mesoscopic diffusive time scales, that is, many orders of magnitude faster than the conventional MD. In this sense, the PFC model would advance to the natural unification of PF and MD modeling approaches.

In Sec. II, a brief description of the MD and PF methods is given. We continue in Sec. III outlining which thermodynamical parameters are transferred from MD to PF method and explain the procedure how they are determined. Results of both methods are compared and discussed in Sec. IV.

II. MODELING METHODS

A. MD simulation model and sample preparation

We perform MD simulations for an isothermal-isobaric (N,T,p) ensemble of N (up to 103 693, with 17 940 Ni) particles and zero pressure. In the whole present work, concentrations c are atomic ones. We use a time step $\Delta t_0 = 2.5 \times 10^{-15}$ s to integrate the equations of motion of the N atoms by means of a fifth-order predictor-corrector algorithm. The temperature is controlled by changing the mean kinetic energy, where a continuous exchange between kinetic and potential energies takes place. The volume of the orthorhombic simulation box, with three-dimensional cyclic boundary conditions, is allowed to fluctuate via Anderson's procedure to realize the zero-pressure condition. Further simulation details are given in Ref. 9.

Interatomic interactions are modeled by the sum of an electronic volume term plus short-ranged pair potentials. For the latter, a Stillinger-Weber form is used, adapted to first-principles interatomic interactions calculated by Hausleitner and Hafner[25] for binary transition-metal alloys. Further details about the potentials parameters can be found in Ref. 9. These quantum-mechanically derived potentials have been calculated within the hybridized nearly free-electron (NFE) tight-binding-bond (TBB) theory, as described in Ref. 25. The structural results from atomistic simulations based on these models are in good agreement with diffraction data, as shown by Hausleitner and Hafner in Ref. 26. Furthermore, these potentials reproduce well the structural trend from polytetrahedral to trigonal prismatic local order in Ni-Zr amorphous, i.e., liquid and glassy, alloys with decreasing Ni content, a topological trend which also is characteristic to the corresponding crystalline compounds. A pronounced similarity of the electronic structure of the crystalline and amorphous phases is also established. The NFE-TBB approach has successfully been extended to other transition-metal amorphous alloys such as Ni-Y, Ni-Nb, Ni-Ti, and Ni-V.[26]

In addition to the structural properties, this interaction model describes fairly well both thermodynamics and dynamics of Ni_cZr_{1-c} alloys. In the case of the intermetallic compound $Ni_{50}Zr_{50}$, e.g., MD modeling yields a cohesion energy of 6.05 eV,[13] which compares sufficiently well with its experimental value of 5.88 eV. The calculated Zr-rich NiZr phase diagram[7] is in good agreement with the experimental diagram,[27] in particular, for the eutectic Zr concentrations of 73% and 63% (experimentally 76% and 64%) and the ratios of melting to eutectic temperatures. The absolute values of these temperatures have, however, to be reduced by about 20% to get an agreement with the experimental values.[13] With respect to the dynamic properties, the experimental diffusion coefficients available in the literature are comparable to those calculated within the MD model used here. Very recent measurements of the mobility of Ni in liquid $Ni_{36}Zr_{64}$ at $T=1700$ K yield $D \sim 2 \times 10^{-9}$ m^2/s,[28] whereas MD-based calculations give $D = 1.6 \times 10^{-9}$ m^2/s for $Ni_{30}Zr_{70}$ at the same temperature. Concerning the glassy state, a fair agreement is also obtained between MD simulation results and experimental ones for $Ni_{50}Zr_{50}$ [simulation: $D_0 = 5 \times 10^{-7}$ m^2/s and $Q = 1.2$ eV (Refs. 29 and 30); experiment: $D_0 = 1.7 \times 10^{-7}$ m^2/s and $Q = 1.3$ eV (Ref. 31)]. Whereby, this last comparison has to be taken with caution in view of the inevitably different degrees of relaxation in glasses achieved in MD simulations (microscopic times, nanosecond to microsecond) and experiments (macroscopic times, seconds to hours).

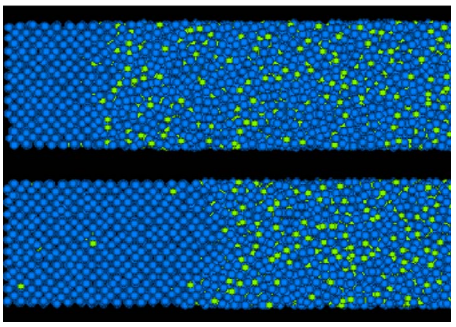

FIG. 1. (Color online) Upper panel: two-phase crystal-melt system equilibrated at $T=1900$ K. Lower panel: the same sample after cooling it down to $T=1700$ K and relaxing it for 20 ns. The hell and dark atoms represent Ni and Zr, respectively. Clearly visible is an expansion of the crystalline fraction on account of the molten part, which implies an increase in the melt concentration $c_l(T)$ under cooling conditions.

In the MD simulations, the two-phase crystal-melt sample is prepared as follows: a bcc Zr crystal is equilibrated at a temperature $T=1900$ K that lies below the melting temperature of the simulation model $T_m^{Zr}=2735$ K. As next, we construct a liquid sample with a yz cross section having the same dimensions Ly and Lz as those of the Zr crystal sample equilibrated before, $Ly=Lz=10$ unit-cell lengths of the bcc Zr crystal. The Cartesian direction x is chosen here orthogonal to the crystal-melt interface.

This liquid probe is first relaxed until equilibration at $T=3000$ K, then quenched down to $T=1900$ K and subsequently equilibrated again. Thereby the length of the liquid cells in y and z directions are held constant at the initial values while the box length along x direction fluctuates to realize the ensemble condition of zero pressure. The yz surface of the bcc Zr crystal is then brought into contact with that of the liquid Ni_cZr_{1-c} sample. Owing to the periodic boundary conditions, two solid-liquid interfaces perpendicular to the x direction are generated in the resulting two-phase sample. This latter is relaxed again at $T=1900$ K until the equilibrium Ni concentration of the melt is reached, here $c_l(1900\ \mathrm{K}) = 0.219(3)$. In order to reduce the equilibration time, the starting composition of the liquid sample is chosen close to the equilibrium value. A change in the melt composition occurs through growing or shrinking of the crystalline part as illustrated in Fig. 1.

A direct MD-based way to determine the liquidus line consists in annealing the two-phase sample at different tem-

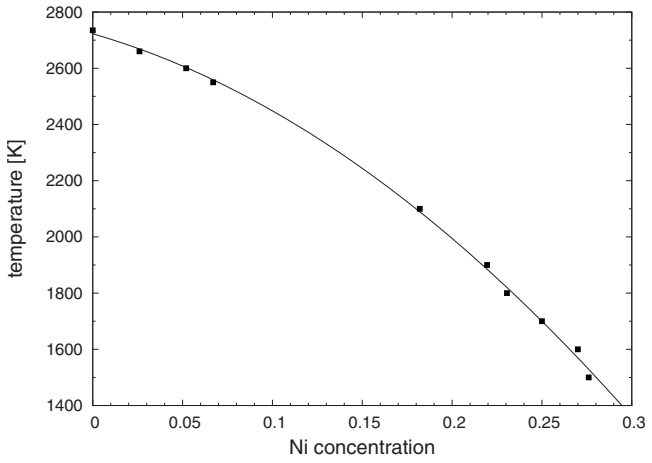

FIG. 2. Zr-rich part of the Ni-Zr phase diagram with discrete MD data points (solid dots) and a second degree polynomial interpolation function.

peratures T to determine the corresponding equilibrium concentrations $c_l(T)$. Figure 2 exhibits the results of these equilibration MD simulations in the range of temperatures between T_m^{Zr} and $T=1500$ K.

Growth and melting dynamics are studied by considering a crystal-liquid layered sample equilibrated at temperature T and brought into a nonequilibrium state by subjecting it to an abrupt positive or negative temperature change ΔT. This corresponds in our case to a supersaturated or undersaturated solution at temperature $T+\Delta T$, respectively. During the subsequent relaxation process at $T+\Delta T$, the system moves in the direction of the equilibrium state by growing or dissolving of its crystalline part (Fig. 1). All the solidification and melting simulations considered below start from a layer sample equilibrated at temperature $T=1900$ K. Propagation of the crystal-melt interface and evolution of the concentration profiles are recorded. In order to model isothermal crystallization and melting conditions, heat production or absorption is compensated by keeping the interfaces and their surroundings at constant temperature. This is assumed in addition to the global temperature control of the system by a Berendsen thermostat. These conditions keep the temperature spatially constant over the whole sample. Such an isothermal assumption is well justified, since, on one hand, the ratio of thermal to chemical diffusivity is typically 10^4 in alloys. On the other hand, we are dealing with a growth kinetics which is dominantly diffusion controlled, as we will show in Sec. IV. Moreover, Hoyt *et al.*[32] have shown, in a free solidification MD simulation of pure Ni and Cu, that the growth velocity was independent of the means of extracting heat from the system even for growth velocities higher than those considered in the present work. This observation has been confirmed by Karma and Rappel[33] from a PF analysis for a pure melt.

For a better statistics of the MD results, each growth or melting simulation is repeated three times, starting from different configurations. The average is then achieved over the six resulting growth or melting fronts.

Another two-phase layer system is constructed to simulate the intermetallic compound $NiZr_2$ in the orthorhombic crystalline structure of type C16. These simulations have the purpose to determine the melting temperature T_m, the latent heat L_m, and the kinetic coefficient μ, parameters needed to calibrate the PF model for a reference system, here $NiZr_2$. The sample preparation procedure is similar to that applied for the intermetallic compound $Ni_{50}Zr_{50}$ in Ref. 13. We start with a crystalline sample, the half of which (along x axis) is molten by heating it at 2000 K while the other half of the lattice is kept at its initial configuration. Then, the whole layer system is annealed at the temperatures of interest for a few hundred picoseconds and subsequently production runs at the same temperature are carried out. Below T_m, the crystal grows while above T_m it melts. T_m is defined as the temperature at which the interface velocity vanishes. Determination of T_m, L_m, and μ are described in Sec. III B. For more details, see Ref. 13.

B. Phase-field model

Different from sharp-interface models of phase transitions, continuously varying order parameters $\phi_\alpha(\boldsymbol{r},t)$ are introduced in the phase-field method. They describe the local volume fraction of the phase associated with the parameter, i.e., $\phi_\alpha=1$ corresponds to a pure α phase, whereas the diffuse interface between two phases is characterized by $0<\phi_\alpha<1$. For this work, we use the thermodynamically consistent multiphase-field model given in detail in Refs. 34 and 35, for which many analytical, numerical, and data postprocessing methods have been developed in the past. Here, evolution equations for the phase fields and (molar) concentrations are derived from the entropy functional defined on the spatial domain Ω,

$$\mathcal{S}=\int_\Omega \left[s(\boldsymbol{\phi},\boldsymbol{c},T)-\varepsilon a(\boldsymbol{\phi},\nabla\boldsymbol{\phi})-\frac{1}{\varepsilon}w(\boldsymbol{\phi}) \right] d\boldsymbol{r}, \qquad (1)$$

which contains separate bulk contributions $s(\boldsymbol{\phi},\boldsymbol{c},T)$ as a function of phase state, composition and temperature, and interfacial entropy density contributions $a(\boldsymbol{\phi},\nabla\boldsymbol{\phi})$ and $w(\boldsymbol{\phi})$, which depend only on the phase-field parameters. Here, ε is a length related to the diffuse interface width. In general, $\boldsymbol{\phi}$ is a vector of N_p phase fields and $\boldsymbol{c}$ a vector of K_c molar concentrations, where N_p and K_c are the number of phases and components in the system, respectively. For the case of NiZr, we reduce the number of field variables to the binary sets $\boldsymbol{\phi}=(\phi_s,\phi_l)$ and $\boldsymbol{c}=(c_1,c_2)$ (1 for Ni and 2 for Zr), bearing in mind the constraints $\phi_l+\phi_s=1$ and $c_1+c_2=1$. In the following, we keep the general multiphase formalism of the model[34] and use two parameters ϕ_l and ϕ_s for liquid and solid phase.

In the derivation of the evolution equations for the phase fields and concentrations, we assume the validity of local thermodynamic equilibrium. If the simulation domain is subdivided into equal sized, constant small volumes V_0 (e.g., the volume of a discretization cell), we can assume thermodynamic potential densities like $s=S/V_0$ for the entropy density in Eq. (1). Using the fundamental relation between internal energy, Helmholtz free energy and entropy $e=f+Ts$, the differential of the entropy density gives

$$ds = \frac{1}{T}de - \sum_{i=1}^{K} \frac{\mu_i}{T} dc_i - \sum_{\alpha=1}^{N} \frac{1}{T}(\partial f/\partial \phi_\alpha) d\phi_\alpha, \tag{2}$$

from which it is clear that $\partial s/\partial e = 1/T$ and $\partial s/\partial c_i = -\mu_i/T$, where $\mu_i = \frac{\partial f}{\partial c_i}$. When restricting ourselves to an isothermal situation assuming a constant undercooling or superheating, the free energy of each phase can be written as a function of the composition only. A general approach is to interpolate the free energy between the two phases in the form

$$\begin{aligned} f(\boldsymbol{\phi}, \boldsymbol{c}) &= f_s(c_1)h(\phi_s) + f_l(c_1)h(\phi_l) \\ &= f_l(c_1) + [f_s(c_1) - f_l(c_1)]h(\phi_s), \end{aligned} \tag{3}$$

where f_α indicates the free-energy density of the respective phase, given as a function of a single concentration only. The function $h(\phi)$ is a suitable interpolation function, for which we use the polynomial $h(\phi) = \phi^2(3-2\phi)$ for all simulations. In Eq. (3), the symmetry property $h(1-\phi) = 1-h(\phi)$, necessary for local energy conservation, has been applied.

From the entropy functional in Eq. (1), assuming local thermodynamic equilibrium, an evolution equation for the molar concentrations c_1 can be derived. According to the linear relaxation ansatz from continuum thermodynamics, the mass fluxes $\mathbf{J}_i$ are written as linear combinations of the thermodynamic driving forces $\nabla \frac{\delta S}{\delta c_i} = \nabla(\frac{-\mu_i}{T})$ ($\delta/\delta c_i$ denotes a functional derivative), e.g., for the first component,

$$\mathbf{J}_1 = L_{11}(\boldsymbol{\phi}, \boldsymbol{c}) \nabla \left(\frac{-\mu_1}{T} \right) + L_{12}(\boldsymbol{\phi}, \boldsymbol{c}) \nabla \left(\frac{-\mu_2}{T} \right). \tag{4}$$

The mobility coefficients L_{ij} obey the Onsager relation and define a symmetric matrix $L_{ij} = L_{ji}$. Owing to the constraint $\Sigma_i c_i = 1$, they also have the following summation property $L_{11} + L_{12} = 0$. A possible choice for L_{11} as proposed in Ref. 34 is

$$L_{11} = \frac{v_m}{R_g} \frac{D_1 c_1 \cdot \kappa D_2 c_2}{D_1 c_1 + \kappa D_2 c_2}. \tag{5}$$

In Eq. (5), v_m denotes the molar volume, R_g the gas constant, and κ the volume ratio of Zr and Ni atoms, $\kappa = v_{\mathrm{Zr}}/v_{\mathrm{Ni}}$. The factor κ has been omitted in the original PF model construction,[34] where for simplicity it was supposed that all atom species have the same atomic volume. For a binary alloy with atom species of different sizes, κ has to be introduced.[36] Phase-dependent diffusivities of the species i are interpolated using the previously defined interpolation function $h(\phi)$ as

$$D_i(\boldsymbol{\phi}) = D_i^s h(\phi_s) + D_i^l h(\phi_l), \tag{6}$$

where D_i^s and D_i^l are the diffusion coefficients of bulk solid and liquid, respectively. The evolution equations for the concentrations are based on the balance of mass. With the property $L_{12} = -L_{11}$ we can thus write for constant temperature

$$\partial_t c_1 = -\nabla \cdot \mathbf{J}_1 = \frac{1}{T} \nabla \cdot L_{11}(\phi_l, c_1) \nabla [\mu_1(c_1) - \mu_2(c_1)]. \tag{7}$$

The concentration [Eq. (7)] is coupled to the actual phase boundary defined by ϕ_α via the mobility coefficient and the chemical potentials μ_i.

When we reduce the model to a single phase-field parameter for the solid ϕ_s, which is sufficient to describe a two-phase problem, the gradient entropy density in Eq. (1) can be chosen as $a(\nabla \phi_s) = \gamma |\nabla \phi_s|^2$ and the potential in the form of a multiwell $w(\phi_s) = 9\gamma \phi_s^2 (1-\phi_s)^2$. The parameter γ in $a(\nabla \phi_s)$ is the solid-liquid interface entropy, which can be defined using the surface tension σ, $\gamma = \sigma/T$. Since only planar front solidification is studied here, no surface energy anisotropy is included in the gradient entropy term.

The evolution equation for the phase fields follows from a local maximization of the entropy functional [Eq. (1)] using a variational approach.[34,35] For the single solid order parameter ϕ_s it reads

$$\varepsilon \tau \partial_t \phi_s = \gamma \varepsilon \nabla^2 \phi_s - \frac{1}{\varepsilon} \frac{\partial w(\phi_s)}{\partial \phi_s} - \frac{1}{2T}(f_s - f_l) \frac{\partial h(\phi_s)}{\partial \phi_s}. \tag{8}$$

τ is a kinetic coefficient that has to be determined for a reference system. As the PF simulations will be restricted to a one-dimensional setting with x as spatial coordinate, all gradients are replaced by the x derivative. The nonlinear PDEs are solved numerically on a regular grid of 5956 grid points using a finite difference scheme with explicit time discretization and cyclic boundary conditions. The grid distance was set to 0.3 Å, leading to a high resolution of the diffuse interface of about 70 grid points. The simulation period for each run comprised 100 ns resolved by a discrete time step of $\Delta t = 1 \times 10^{-15}$ s.

III. THERMODYNAMIC AND KINETIC DATA FROM MD SIMULATIONS

A. Entropy and free energy of Zr-rich Ni_cZr_{1-c} from MD simulations

Understanding of the crystallization process of alloy melts requires the knowledge of the chemical potentials of the involved phases, as they are the driving forces for a phase transition. This means that we need to determine the temperature- and concentration-dependent FE of the different phases. This task is not obvious for liquids by means of atomistic modeling, contrarily to crystals for which it is relatively easily tractable. The difficulty resides in the fact that there is no direct way to enumerate all possible configurations of the disordered liquid structure, and hence to calculate the entropy and related thermodynamic properties such as the FE. The concept of defects cannot unambiguously defined for liquids, as is the case for crystals. Energy or enthalpy values are, however, easily accessed to from the interatomic potentials.

In the following, we summarize the MD-based method developed by Küchemann and Teichler[7,8] to evaluate the free energy and the entropy of binary mixtures, applied here for

the Zr-rich metallic NiZr alloy. This method is described in details in Ref. 7.

The method consists of two steps: (a) calculation of entropy and FE for two reference crystalline compositions, in this study the intermetallic compounds $Ni_{50}Zr_{50}$ and $NiZr_2$. (b) Calculation of the entropy and FE of Ni_cZr_{1-c} for arbitrary composition c using results of the reference systems in (a).

In the case of perfect (without defects) crystalline phases, at sufficient low temperature T_0, the entropy can well be approximated by the vibration entropy s_{vib}. To calculate s_{vib}, we need the vibration density of state. Here it is calculated by taking the Fourier transform of the velocity correlation function.[37] The entropy of the melt follows by integrating $ds=\frac{C_p}{T}dT$ from T_0 to $T>T_m$, using $s_{vib}(T_0)$ as initial value. T_m is the melting temperature and C_p means the specific heat of the crystal or melt, a quantity deduced from the slope of energy data as function of temperature $e(T)$. The singular melting entropy $\Delta s_m=\frac{L_m}{T_m}$ also has to be considered, L_m being the latent heat (the energy jump at T_m). Entropy $s(T)$ and energy $e(T)$ give then the FE $f=e-Ts$.

The special feature in the method developed by Küchemann and Teichler is its ability to deduce the entropy and FE of the melt for arbitrary composition c, regardless of the existence of a crystalline structure at this composition. The change in the chemical potential with composition, $\partial_c[\mu_{Ni}(c,T)-\mu_{Zr}(c,T)]$ is derived from analyzing the spatial variation in Ni concentration c under the influence of a spatially varying auxiliary potential acting on Ni atoms. Using the relation $\partial_c^2 f(c,T)=\partial_c[\mu_{Ni}(c,T)-\mu_{Zr}(c,T)]$, yields $f(c,T)$ by integrating the latter equation twice with respect to c. Finally, the resulting two integration constants are determined by using the FEs calculated before for the two reference compositions $c=0.5$ and $c=0.33$. The approach above has to be applied only for one given temperature T_r. The FE $f(c,T)$ at an arbitrary temperature T is obtained through a quite simple thermodynamic integration between T_r and T, for which the specific heat of melt $C_{p,liq}(c,T)$ and of crystal $C_{p,cryst}(c,T)$ are needed. Both are accessible from the c and T dependence of the energies.

Figure 3 presents FE values of Ni_cZr_{1-c} melts at $T=1700$ K (crosses) as evaluated within the MD-based thermodynamic approach of Küchemann and Teichler. The figure includes the FE of the bcc Zr crystal at very low Ni concentrations (squares). Application of the double tangent construction, as represented in Fig. 3 by the dashed-dotted line, leads to the equilibrium liquid and solid concentrations in a $[Ni_cZr_{1-c}]_{liquid}$-$Zr_{crystal}$ layer system, that is, the liquidus line between melt and crystalline Zr and the solubility line of bcc Zr, respectively. Since a continuous function of the FE will be needed for the PF model, we interpolate the calculated FE values with a third-order polynomial (solid line).

The concentration across the crystal-liquid interface region varies between the equilibrium concentrations c_s and c_l of coexisting solid and liquid phases, respectively. In the PF model, the FE at the interface for an intermediate concentration c_I, $c_s<c_I<c_l$, is defined as combination of the FEs of the coexisting phases with a suitable weighting function [see Eq. (3)], whereby we implicitly suppose that the FEs of solid and liquid are defined at each c_I value. In the case of the often used classical regular solution model, this assumption is verified per construction of the model. In our MD model, the liquid phase exists over the whole concentration range. While for the Zr crystal, MD experiments reveal that the crystal with homogeneously solved Ni atoms exists as such only up to a certain Ni solubility limit, about 2% at 1700 K. Beyond this limit, Ni atoms start to segregate in small Ni enriched clusters within the Zr matrix and one can no longer speak of a homogeneous single crystalline solution but rather of a new two-phase system. Estimation of the FE for this new phase needs the elaboration of new approaches that are outside the scope of our present study.

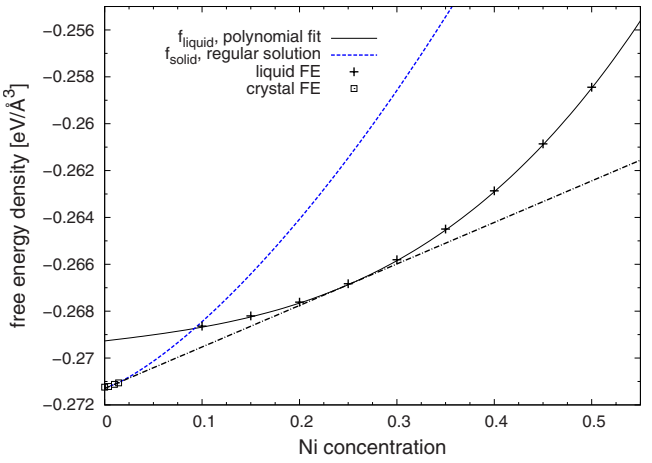

FIG. 3. (Color online) Crosses: MD-calculated FE density for Zr-rich Ni_cZr_{1-c} melts at $T=1700$ K, the solid line is a third-order polynomial interpolation function. Squares: MD-calculated FE density for crystalline Zr at low Ni concentrations (<2%), the dashed line extrapolates these values to higher concentrations according to the regular solution model, see text for details. The dashed-dotted line is the double tangent.

For the need of the PF modeling, we use for the crystalline phase the regular solution approximation[38] in order to extrapolate the FE values, calculated for the narrow range of low Ni solubility, to higher Ni concentrations,

$$e_{cryst}=ce_{Ni}+(1-c)e_{Zr}+c(1-c)h_{NiZr}, \tag{9}$$

$$s_{cryst}=s_{Zr}^{vib}+R_g[c\ \ln(c)+(1-c)\ln(1-c)], \tag{10}$$

$$f_{cryst}=e_{cryst}-T\cdot s_{cryst}, \tag{11}$$

where e_i is the energy of the pure element i (i=Ni and Zr), from MD simulations (Table I). h_{NiZr} is the Ni-Zr interaction parameter that we suppose to be concentration independent

TABLE I. FE parameters of crystalline Zr.

T (K)	e_{Zr} (eV)	e_{Ni} (eV)	h_{NiZr} (eV)	s_{Zr}^{vib} (meV/K)
1700	−5.815	−3.650	−1.041	0.884
2100	−5.707	−3.608	−1.011	0.941

but temperature dependent. In order to calculate h_{NiZr}, we equalize the energy values determined by MD simulation for low Ni concentrations, where the homogeneous crystal phase still exists, with the right side of Eq. (9). By averaging over three concentration values, we found $h_{\mathrm{NiZr}}=-1.041$ eV/atom at $T=1700$ K and $h_{\mathrm{NiZr}}=-1.011$ eV/atom at $T=2100$ K. s_{Zr}^{vib} is the vibrational entropy of the crystal approximated by that of pure crystalline Zr from Ref. 7. The second term of Eq. (10) is the standard entropy of mixing. The dashed line in Fig. 3 illustrates the results of this approximation for f_{cryst} at $T=1700$ K.

B. Crystal-melt interface properties and atomic size ratio

Experimental access to the crystal-liquid interface remains a challenging task due to the difficulties of designing experiments that are sensitive only to the interfacial region whose width is limited to a few atom sizes. Therefore, atomistic modeling (e.g., MD or Monte Carlo) has recently advanced to an alternative method in providing PF models with interface parameters.

MD simulations reveal that a crystal-melt interface is a diffuse region where interpenetration of crystal and melt takes place over several atom sizes. An approximate width can be assigned to the interface as the extension of the region over which a given atomic order-parameter profile varies from a bulk solid value to a bulk melt one. We use the local order parameter Q_6, introduced by Steinhardt *et al.*,[39] because of its high sensitivity in discriminating crystalline and liquid atomic environment. Fitting the Q_6 profile with a suitable analytical expression yields the interface thickness $2\varepsilon \simeq 12$ Å. Further details can be found in our earlier work.[6]

At the preliminary stage of our work, we carried out PF simulations in order to test how sensitive the model is to the different thermophysical parameters, and hence to know with which degree of accuracy these parameters have to be determined. For the surface energy σ we started with a value typical for metallic systems and established that σ can be varied by a factor 0.1 up to 10 without any significant influence on the PF simulation results. This observation will be discussed in Sec. IV. Therefore, there is no need, in the case of planar solidification, to accurately determine σ for $[\mathrm{Ni}_c\mathrm{Zr}_{1-c}]_{\mathrm{liquid}}$-$\mathrm{Zr}_{\mathrm{crystal}}$ interfaces (e.g., by means of MD methods). A value typical for NiZr alloy is largely sufficient. Two values are known in the literature that of pure Zr with $\sigma=0.16$ J/m^2 and of pure Ni with $\sigma=0.30$ J/m^2.[40] Since we are operating in the Zr-rich region of $\mathrm{Ni}_c\mathrm{Zr}_{1-c}$ alloy, we use the first value.

For calculating the coefficient $\tau=\frac{L_m}{\mu T_m^2}$ of Eq. (8), we use the melting temperature T_m, the latent heat L_m, and the kinetic coefficient μ of the intermetallic compound NiZr_2, which is the crystalline structure closest to the concentration range we are considering in this work. We use the values $T_m=1610$ K and $L_m=0.201$ eV/atom determined by Küchemann[7] using an approach based on simulating the time evolution of a crystal-melt layer within an isenthalpic ensemble (N,H,p). The kinetic coefficient μ represents the constant of proportionality between the velocity of the interface propagation v_I and the undercooling $\Delta T=T_m-T$ around T_m. In order to determine μ for NiZr_2, We apply the free solidification technique as in Ref. 13 for $\mathrm{Ni}_{50}\mathrm{Zr}_{50}$. Accordingly, a two-phase layer system is quenched to a temperature T and allowed to solidify $(T<T_m)$ or to melt $(T>T_m)$. A fit of the relation $v_I=\mu\Delta T$ yields the kinetic coefficient $\mu=0.082$ m/s K.

The atomic size ratio can be estimated by using the partial radial distribution functions g_{NiNi} and g_{ZrZr} calculated within the present MD model[41] for the NiZr melt. Identifying the first peaks of these functions with the Ni-atom and Zr-atom diameters, respectively, we obtain $\kappa^{-1/3}=R_{\mathrm{Ni}}/R_{\mathrm{Zr}}=0.755$. This estimated value of κ is in the range of that calculated in terms of the experimental atomic radii of the pure metals $\kappa_{exp}^{-1/3}\in[0.76,0.78]$.

C. Diffusion coefficients

The diffusion equation [Eq. (7)] is one of the two central evolution equations in the PF model. The diffusion coefficients of the different phases are key parameters that have to be determined by other methods. Experimental data for diffusion in the liquid phase and at the crystal-liquid interface are lacking for most of the materials. MD-based methods are a valuable help to remedy this lack.

We determine the one-dimensional diffusion coefficients $D_{\mathrm{Ni,Zr}}$ by monitoring the asymptotic limit of the mean-square displacement (MSD) in the growth direction x,

$$D_{\mathrm{Ni,Zr}}=\frac{1}{2t}\lim_{t\to\infty}\partial_t\langle(r_x^i(t_0+t)-r_x^i(t_0))^2\rangle_{i,t_0}, \tag{12}$$

where $r_x^i(t)$ is the x coordinate of particle i at time t. The average is performed over particles i and reference time t_0. The MSD is measured until a time t^*, at which the asymptotic linear regime is reached. t^* corresponds to a few picoseconds at $T=1700$ K for Ni atoms in both phases and for Zr atoms in the melt phase (compare with data of Mutiara and Teichler in Ref. 9 for $\mathrm{Ni}_{20}\mathrm{Zr}_{80}$). In the case of Zr atoms in the bulk Zr crystal, the diffusion is too small to be measured effectively within the time available for MD simulations. Even after 100 ns, the MSD still exhibits the typical vibrational behavior. This means that diffusion of Zr atoms in the crystal can be neglected in our case. For the need of the PF simulation, we use the lowest value of diffusion coefficient we are able to accurately determine by MD simulations within the available simulation time of about 100 ns. We estimate this lowest value to $D_{\mathrm{Zr},cryst}\simeq 10^{-12}$ m^2/s. Setting $D_{\mathrm{Zr},cryst}$ to even lower values leads to the same results. In PF modeling, one considers the phase dependence of diffusivity by interpolating the bulk diffusion coefficients in solid and liquid according to Eq. (6). The variation in diffusivity within a phase is thereby neglected. The concentration dependence concerns only the free-energy density [Eq. (3)]. We determined bulk diffusivities by considering atoms far from the interface during a growth or melting simulation. The average is done over a large number of atoms and initial configurations so that the statistical uncertainty lies in a range of a few percents. The obtained values, given in Table II, from a two-phase system are the same as those calculated for one-phase systems (solid or liquid separately) at the ini-

TABLE II. Diffusion coefficients from MD simulation (unit: 10^{-9} m^2/s).

T (K)	$D_{Ni,liq}$	$D_{Ni,cryst}$	$D_{Zr,liq}$	$D_{Zr,cryst}$
1700	1.74 ± 0.05	13.30 ± 0.83	0.893 ± 0.020	0.001
2100	4.30 ± 0.09	15.70 ± 0.90	2.36 ± 0.05	0.001

tial concentrations c_s^0 and c_l^0, which are the equilibrium concentrations of a two-phase system at the initial temperature (Table III).

In order to take an insight into the nonobvious behavior of the atom mobility when crossing from one phase into the other, we calculate the diffusion profiles $D_{Ni}(x)$ and $D_{Zr}(x)$ during a crystallization experiment. This is achieved by averaging the diffusion coefficient over all particles that belong at the reference time t_0 to one slice situated at $(x, x+\Delta x)$, where each slice has a thickness of about $\Delta x = 3$ Å. Since the particles can move from a layer to another, we choose t^* such that about 90% of the atoms belonging to a given slice k at t_0 stay in the same slice or move to a nearest-neighbor one $(k \pm 1)$ during t^*. We found no significant difference between this x-direction diffusion profile and that of the lateral (yz) diffusion calculated in our recent work.[6] Figures 4 and 5 illustrate the diffusion profiles of both atom species at $T = 1700$ K and $T = 1300$ K, respectively, recorded 40 ns after having quenched the system down from $T = 1900$ K. The small decrease in the Ni diffusivity ahead of the interface (liquid side) results from the confinement effect due to the crystalline wall. This effect is also observed in systems under equilibrium conditions and becomes more pronounced with decreasing temperature. The concentration variations at the interface during the growth and dissolution induce a similar effect on the diffusion coefficients but this can be neglected relative to the confinement effect.

The noise in the crystalline region is caused by the poor statistics owing to the very small solubility of Ni atoms in the Zr crystal ($c_s \simeq 0.01$). We observe a higher mobility of Ni atoms in the bcc Zr crystal than in the melt at the considered temperature. To explain this somehow unusual feature, we have to compare the environment of Ni in both regions. In the melt, Ni atoms are confined in cages, which are the same as those building the intermetallic phases NiZr (B33-Type with Ni-centered trigonal prisms as structural units) and $NiZr_2$ (CrB-Type with Archimedean antiprisms as structural units).[37] These structural units are dictated by the nature of the interatomic interactions when building the crystalline phases. They are obviously more stable, and thus restrict the Ni atoms more effectively, than the octahedral sites encountered by Ni atoms in the bcc Zr crystal. Such an anomalously fast diffusion of Co, Ni, and Fe in the β phase (bcc structure) of pure Zr and other transition metals (e.g., Ti and Hf) has been reported in earlier works.[42] While experimental Ni diffusivity in NiZr melt is meanwhile available, no data of Ni diffusivity in β-Zr are known to us. This makes difficult to provide a direct proof for the anomalous diffusion feature observed in our MD simulations. Nevertheless, the following observations corroborate the assumption that this feature is a real effect and not an artifact of the used MD model. The diffusivity of α-Zr (fcc) can be extrapolated from low-temperature measurements[43] to between 10^{-8} and 10^{-7} m^2/s at $T = 1700$ K, a value which is at least one order higher than the experimental diffusivity of Ni in liquid $Ni_{36}Zr_{64}$ (Ref. 28) (see Sec. II A). Since α-Zr is closer packed than β-Zr, the diffusivity in the latter is expected to be even higher than the extrapolated value for α-Zr. Moreover, the diffusivity of Ni at $T = 523$ K (Ref. 44) is found to be at least 10^4 smaller in amorphous $Ni_{50}Zr_{50}$ than in crystalline Zr. This is another manifestation of the anomalous fast diffusivity of Ni in crystalline Zr. Due to its high free volume, the disordered amorphous structure is expected to rather have a higher diffusivity than the crystal.

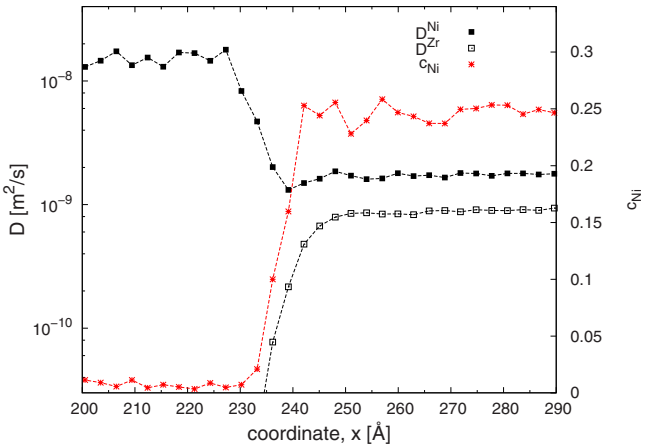

FIG. 4. (Color online) Diffusion profiles for Ni and Zr around the crystal-liquid interface at $T = 1700$ K, recorded 40 ns after quenching the system down from $T = 1900$ K. The corresponding concentration profile is also shown.

IV. RESULTS AND DISCUSSION

Figure 6 shows the Ni-concentration profile across the solid-melt interface during a MD isothermal solidification simulation at $T = 1500$ K. This undercooling value—starting from 1900 K—gives the highest growth velocity (see Fig.

TABLE III. Phase-field simulation parameters determined from MD simulation. c_s^0 and c_l^0 are the solid and liquid equilibrium concentrations, respectively, of a two-phase system at the initial temperature $T_i = 1900$ K.

ε (Å)	τ (eV ns/Å^4 K)	σ (eV/Å^2)	c_s^0	c_l^0	κ
6.0	3.505×10^{-9}	0.010	0.0084	0.2193	2.32

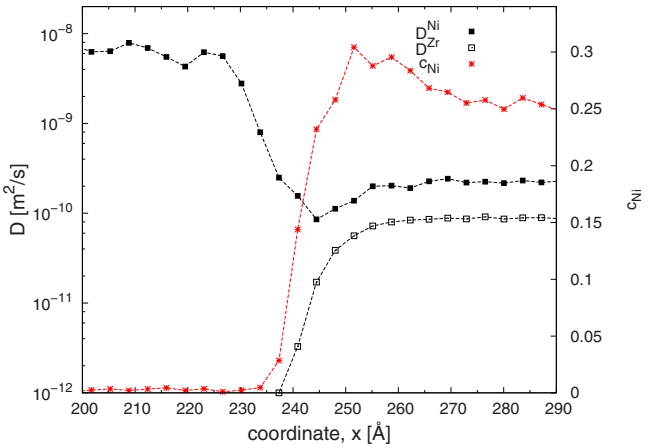

FIG. 5. (Color online) Diffusion profiles for Ni and Zr around the crystal-liquid interface at $T=1300$ K, recorded 40 ns after quenching the system down from $T=1900$ K.

10). We observe that after a few nanoseconds the liquid concentration at the interface reaches a value which fluctuates around the equilibrium concentration of the final temperature, $c_l(1500\ \mathrm{K})=0.276(5)$, during the whole growth process. We can conclude that, at the growth velocities considered in our MD simulations, the equilibrium conditions can be assumed to prevail in the liquid phase at the immediate vicinity of the interface. This point is important when comparing results of MD and PF methods since the latter approach produces per construction exactly the concentrations at the interface as derived from the common tangent applied to the equilibrium FE versus concentration. The MD approach gives rise to the same equilibrium concentrations only at sufficiently low growth velocities, as is the case in the present study. At high velocities, the interface concentration may deviate from the equilibrium one. The atoms have not enough time to be dragged from the interface, they are then trapped into the crystal. This effect can be taken into

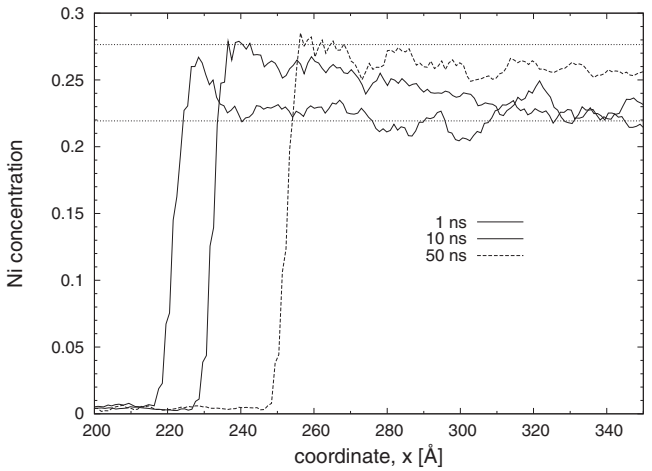

FIG. 6. Evolution of the concentration profile during MD isothermal solidification simulation at $T=1500$ K after undercooling from $T=1900$ K. The horizontal dotted lines represent the equilibrium concentrations at the temperatures $T=1500$ K (upper line) and $T=1900$ K (lower line).

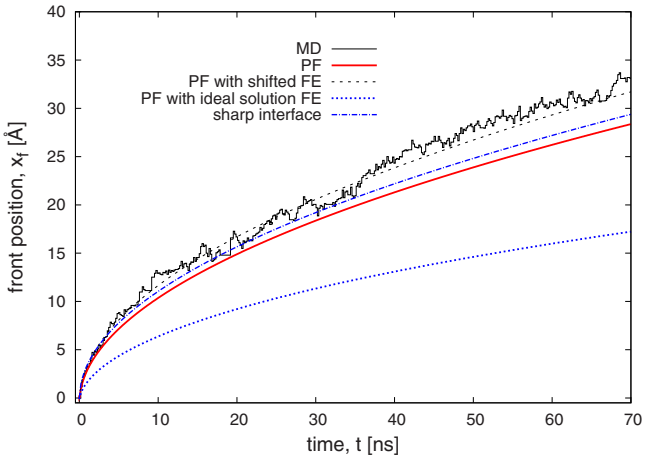

FIG. 7. (Color online) Interface position as a function of time during a solidification process at $T=1700$ K, starting from a two-phase system equilibrated at $T=1900$ K (see snapshot of Fig. 1). The diagram compares results from MD, PF, and sharp-interface models.

account by the inclusion of suitable terms in the FE functional of the PF model.[11]

Figure 7 displays the evolution in time of the front position at $T=1700$ K after undercooling the sample from $T=1900$ K for both modeling methods. Figure 8 represents the corresponding Ni-concentration profiles after 20 ns of the solidification process. The agreement between MD and PF modeling is very satisfactory. A good matching concerns also the height of the concentration peak at the interface, with the values $c_{l,I}^{\mathrm{MD}}=0.250$ and $c_{l,I}^{\mathrm{PF}}=0.246$, both corresponding to the liquid equilibrium concentrations (at $T=1700$ K) of the respective modeling methods. Broadening of the concentration peaks toward the bulk liquid and the Ni solubility of the Zr crystal in the MD simulation are well reproduced by the PF simulation. We can conclude that the PF model we constructed recovers quite well the relaxation dynamics toward

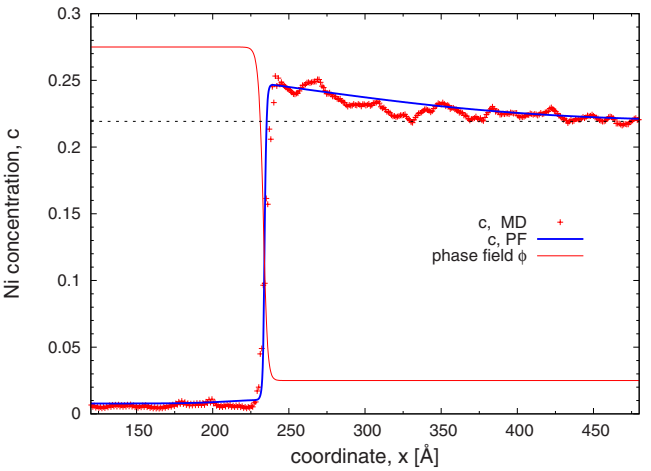

FIG. 8. (Color online) Ni-concentration profiles after 20 ns of a solidification process, from the same MD and PF simulations described in Fig. 7. The dashed line indicates the initial liquid equilibrium concentration $c_l^0=c_l(1900\ \mathrm{K})$. The thin solid line corresponds to the diffuse PF profile.

equilibrium of the MD simulations. This result is not obvious keeping in mind that only physical parameters describing equilibrium conditions have been transferred from the MD to the PF model.

We also find a good concordance between the solid-liquid interface as described by the ϕ profile and the interface following from the concentration profile in the PF simulations (Fig. 8). This is a hint that the interpolated interface free energy of Eq. (3), formulated as a phenomenological construction from the calculated FE of liquid and the approximated FE of crystal, describes in a reasonable way the induced free-energy barrier of the transient interface region.

The slightly slower solidification rate in the PF simulation can be explained by the small discrepancy between the equilibrium liquid concentration at 1700 K realized in MD simulations, $c_l^{\mathrm{MD}}(1700\ \mathrm{K})=0.250$, and that following from the calculated FE by means of the common tangent construction, $c_l^{\mathrm{PF}}(1700\ \mathrm{K})=0.246$. As a consequence, the height of the concentration peak at the interface (liquid side) during solidification is about 13% smaller in the PF than in MD simulation (Fig. 8). This corresponds to a smaller gradient of the chemical potential at the solidification front, and thus to a slower solidification kinetics. The PF model approach gives the possibility to verify this assumption since we can "by hand" shift the liquid FE curve $f(c,1700\ \mathrm{K})$ in Fig. 3 vertically upward so that the calculated equilibrium liquid concentration matches with the MD one, i.e., $c_l^{\mathrm{MD}}=0.250$. Using the shifted liquid FE function in the PF simulation leads indeed to a yet better matching between PF and MD modeling, as illustrated by the dashed line in Fig. 8.

The dotted line in Fig. 7 represents the propagation of the front position for an ideal solution formulation of the FE density,[6] an approximation that is often used in estimating the FE density of the liquid phase in PF modeling. The ideal solution approximation leads to a discrepancy between MD and PF modeling, equivalent to a difference of nearly factor 4 in the diffusion coefficients, as discussed in Ref. 6. The ideal solution model neglects any enthalpy of mixing, whereas the MD model yields, for instance, $\Delta H_{mix}=-24.9$ kJ/mole for liquid $Ni_{25}Zr_{75}$ at $T=1700$ K. This value compares well with the experimental measurement by Witusiewicz and Sommer,[45] $\Delta H_{mix}^{exp}\simeq -23$ kJ/mole for the same concentration and at $T=1565$ K. Due to this strong negative enthalpy of mixing characteristic for NiZr systems, the ideal solution model is not able to describe the solidification dynamics in these alloys.

The chemical concentration gradient at the interface toward bulk liquid affects the diffusivity through the thermodynamics of mixing of the NiZr solution. This effect is omitted by the ideal solution model. To quantify this effect let us consider the simple approximation of a dilute regular solution.[38] In this case, the thermodynamic effects which express the deviation from the ideal solution can be taken into account by scaling the solute diffusion coefficient with a factor $\Phi=1-\frac{2\Delta H_{mix}}{R_g T}$. Φ is called the thermodynamic factor, where $\Phi=1$ corresponds to the ideal solution case. The above MD-calculated ΔH_{mix} leads to a thermodynamic factor of $\Phi=4.5$ at $T=1700$ K. This rationalizes the missing factor 4 between the effective diffusion coefficients of MD and PF modeling when the FE density of liquid is approximated on the basis of the ideal solution model. In an experimental study of amorphous Ni-Zr, Karpe *et al.*[46] reported an even stronger effect of the mixing enthalpy on the thermodynamic enhancement of interdiffusivity, with a thermodynamic factor up to 33 ± 8 for a-$Ni_{57}Zr_{43}$ at 623 K.

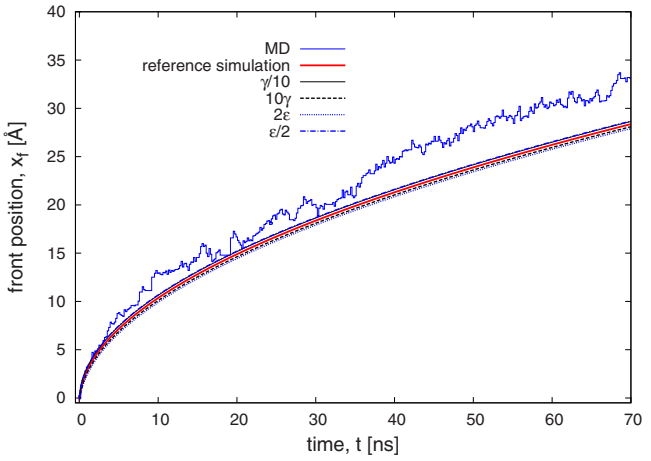

FIG. 9. (Color online) Sensitivity of the PF growth velocity to variation in σ and ε with the same undercooling conditions as in Fig. 7. The results of each parameter modulation is compared with the reference simulation of Fig. 7.

We showed in an earlier work that the strong negative heat of mixing manifests itself in the structural and dynamic properties of NiZr liquid under equilibrium conditions.[47] A pronounced short-range order (SRO) is observed for this liquid system in MD simulations and experiments.[26] Well-defined structural units, similar to those in the corresponding crystalline structures, develop in the liquid at relatively high temperatures.[37] The correlation between these building units explains the observation of an additional sharp diffraction peak, the so-called prepeak, in the static structure factors. In an ongoing MD study on the properties of $[Ni_cZr_{1-c}]_{\mathrm{liquid}}$-$Zr_{\mathrm{crystal}}$ interface, we give evidence that the pronounced SRO in the bulk liquid transforms into a massive lateral ordering at the interface, because of the commensurability between the structural units of the liquid, mainly trigonal prisms, and the periodic potential of the crystalline wall. This ordering affects the atoms mobility near the interface.[48]

Compared with MD methods, PF modeling has the advantage to allow quantitative analysis of how a given physical parameter separately contributes to the growth process. This possibility is not given in MD modeling since all contributions are postulated to reside in the interatomic interaction and each change in the latter one will probably alter all contributions at once. However, after MD modeling has provided the PF model with the necessary physical parameters, it benefits from this model to resolve the role of each parameter independently. In our study, we conducted additional PF simulations to separately vary the magnitude of the interface energy σ and the interface width ε. As represented in Fig. 9, varying the magnitude of the interface energy σ by a factor 0.1–10 is found to have no significant influence on the results. The same conclusion concerns the interface width ε by doubling or halving its value in the PF simulations. This is a

clear hint that the interface properties play a secondary role in determining the growth kinetic in a planar solidification. The dominating weight is assigned to the mass transport from the interface toward the bulk liquid. Diffusivity and thermodynamics of mixing in the NiZr solution affect the speed of this mass transport, as discussed above in regard to the thermodynamic factor. Such a growth mode is termed diffusion limited to distinguish it from the collision-limited one. In the latter, rearrangements of the local structure of the liquid atoms at the interface[19] determine the growth rate and not the long-ranged diffusion of the atoms. This behavior applies to the growth from the melt for monatomic materials. It is worth noticing that for binary intermetallic compounds, although no mass transport (at least not the long-ranged one) is needed for crystallization, diffusion seems to be a determinant factor for the growth rate, as shown by Kerrach *et al.* in the above cited MD study of Ref. 21. This feature calls for further simulations, atomistic as well as mesoscopic, to be elucidated.

Two further investigations corroborate the diffusion controlled character of the growth process of the undersaturated NiZr solution: the sharp-interface analysis and the study of the dependence of the growth rate on the crystal orientation. Due to the negligible influence of the interface properties in the growth process compared to the long-ranged diffusion in the liquid, we expect that the physics in the present case can be treated by the traditional sharp-interface model. The latter is considered as a limit of the PF approach when diffusion lengths are much greater than the crystal-liquid interface. In the one-dimensional sharp-interface model, isothermal solidification of a binary alloy is described by solute diffusion in each phase. This can be as expressed as

$$\frac{\partial c}{\partial t} = \frac{v_m D}{R_g T}\frac{\partial}{\partial x}\left[c(1-c)\frac{\partial}{\partial x}\frac{\partial f}{\partial c}\right], \tag{13}$$

following from the mass balance equation $\frac{\partial c}{\partial t}+\nabla J=0$, where the diffusion flux J of Ni atoms in the melt is given in terms of the driving force $\nabla\frac{\partial f}{\partial c}$ for the diffusion. In a one-dimensional setting, the diffusion flux reads

$$J = -\frac{v_m D}{R_g T}c(1-c)\frac{\partial}{\partial x}\frac{\partial f}{\partial c}, \tag{14}$$

where D is the diffusion coefficient of the solute Ni atoms and f is the temperature- and concentration-dependent FE density of the melt. D and f are the same MD determined quantities used before in the PF modeling. Owing to the very low Ni concentration in the solid and the high Ni diffusivity, we can assume that the solid equilibrium concentration $c_s(T_f)$ of the final temperature T_f is instantly reached in the whole crystal after setting the temperature drop ΔT. Therefore, we set the condition: $c=c_s(T_f)$ for $x<x_f$, where $x_f(t)$ is the position of the crystal-melt interface. This is the case of a one-sided sharp-interface problem.

The interfacial boundary conditions are formulated in terms of the concentrations at the interface according to MD modeling. We write

$$c|_{x=x_f} = c_{l,I}(T_f) = c_l(T_f), \tag{15}$$

$$-\frac{v_m D}{R_g T}c(1-c)\frac{\partial}{\partial x}\frac{\partial f}{\partial c}\bigg|_{x=x_f} = \Delta c V(t), \quad \Delta c = c|_{x=x_f} - c_s(T_f), \tag{16}$$

where $V(t)$ is the growth velocity decreasing to zero with time as the concentration profile at the interface is broadening. For $T_f=1700$ K, we have $c_s(T_f)=0.0078$ in the crystal and $c_{l,I}(T_f)=0.250$ at interface.

The far-field boundary condition is

$$c|_{x\to\infty} = c_l^0 \tag{17}$$

with c_l^0 being the equilibrium concentration of the liquid at the initial temperature $T_i=1900$ K, i.e., $c_l^0=c_l(1900\ \mathrm{K})$ (see Table III).

For the numerical integration of Eqs. (13)–(17), it is convenient to adopt a moving frame

$$z = x - x_f(t) = x - \int_0^t V(\tau)d\tau, \tag{18}$$

where the crystal-melt interface is located at $z=0$. In the moving frame, the diffusion equation in the melt is

$$\frac{\partial c}{\partial t} - V\frac{\partial c}{\partial z} = \frac{v_m D}{R_g T}\frac{\partial}{\partial z}\left[c(1-c)\frac{\partial}{\partial z}\frac{\partial f}{\partial c}\right] \tag{19}$$

and the interface velocity follows from the boundary condition in Eq. (16). This yields

$$V = -\frac{1}{\Delta c}\frac{v_m D}{R_g T}c(1-c)\frac{\partial}{\partial z}\frac{\partial f}{\partial c}\bigg|_{z=0}. \tag{20}$$

The evolutions [Eqs. (19) and (20)] are solved numerically on a regular one-dimensional grid using finite differences with semi-implicit time discretization.

The dashed-dotted line in Fig. 7 represents the solution of the sharp-interface model using the boundary conditions and physical parameters proposed by the MD simulation. The good agreement between the MD result and the sharp-interface solution confirms the diffusion controlled nature of the solidification process of the undersaturated NiZr solution.

Figure 10 exhibits the MD-determined growth rate as a function of the undercooling ΔT for two orientations of the bcc crystal, the (100) and (110) orientations. No significant anisotropy effect on the growth rate can be observed within the calculation accuracy. In the case of a purely collision-limited growth, one expects a growth rate proportional to the distance between two successive atoms layers of the crystal,[49] that is, a factor $\sqrt{2}$ between (100) and (110) orientations for a bcc structure. The increasing deviation of PF results from MD with increasing undercooling is another proof of the essential role of diffusion in the growth kinetics. The confinement effect induced by the crystalline wall at the liquid side of the interface, as described in Sec. III C, becomes more important as the temperature decreases. This effect is equivalent to a diffusivity drop at the interface and is not taken into account in our PF model, which in turn overestimates the growth rate for these conditions. In the construction of the phase-dependent diffusivity in Eq. (6), we make use of the standard method to interpolate the bulk dif-

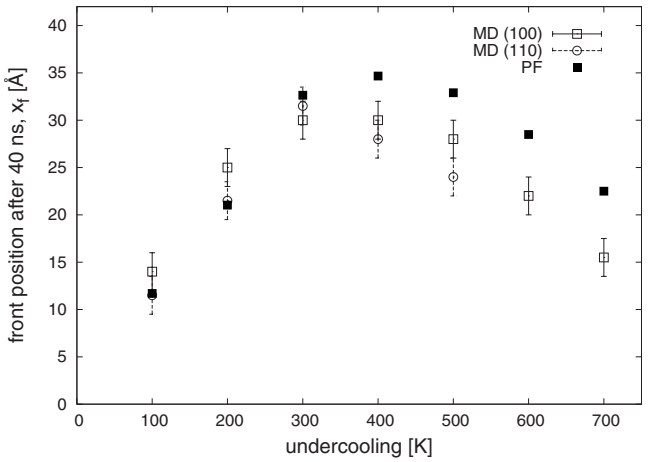

FIG. 10. Front position x_f after 40 ns of solidification as a function of undercooling ΔT for MD and PF simulations. The initial temperature is $T=1900$ K for all simulations.

fusion coefficients in solid and liquid by means of the interpolation function $h(\phi)$. This simple construction seems to be sufficient at high temperatures but it fails as the temperature decreases.

We test the equivalence between MD and PF treatments for the melting kinetics as well. Figures 11 and 12 display the results of simulations with both approaches for a melting experiment. We start thereby from the same initial two-phase sample at $T=1900$ K as before and overheat it by 200 K above the liquidus line. The agreement between PF and MD modeling obtained for the melting process is as satisfactory as in the case of solidification. The slightly faster melting in PF simulation may be traced back to the same reason as in the solidification experiment. The concentration drop at the interface is slightly higher in the PF than in the MD simulation (Fig. 11) leading subsequently to a faster melting kinetics. Similarly to solidification, a better matching is achieved between MD and PF modeling for shifting the calculated liquid or solid FE curve at 2100 K in vertical direction so that the equilibrium liquid concentration matches with the

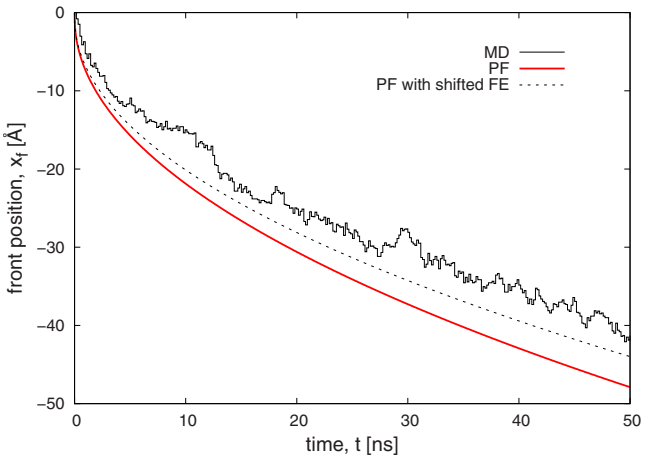

FIG. 11. (Color online) Interface position as a function of time for a melting process at $T=2100$ K starting from the same two-phase samples as in Fig. 7.

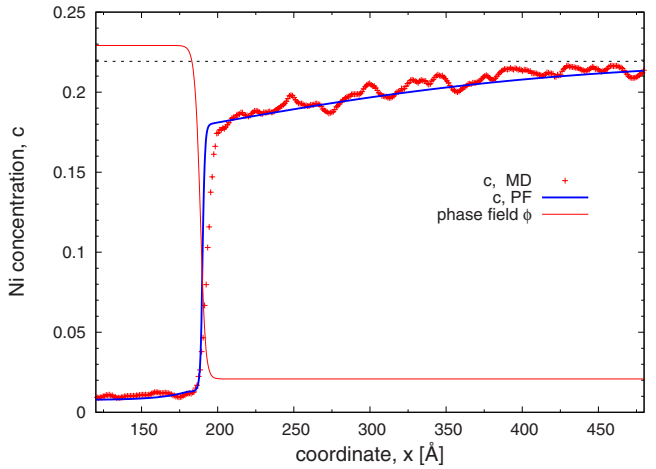

FIG. 12. (Color online) Ni-concentration profiles after 20 ns of a melting process from the same MD and PF simulations as in Fig. 11. The dashed line indicates the initial liquid equilibrium concentration $c_l^0=c_l(1900\ \mathrm{K})$ and the thin solid line illustrates the profile of the PF variable ϕ.

MD result. This observation raises two issues related to the calculated FE by means of MD methods that have to be investigated in the future as potential sources of the described small discrepancies between MD and PF methods. The first issue concerns the accuracy of the FE calculations for crystalline and liquid NiZr binary alloy.[7] The second issue is addressed to the relevance of approximating the FE density of the crystal at high Ni concentrations, where the homogeneous crystal does not exist. In forthcoming studies, other approaches should be recalled to construct the FE density of the interface, particularly those which better reflect the morphology of the interfacial region than the method we use in the present work. We consider the interface as a mixture of two phases with identical concentrations varying from the bulk liquid concentration to the bulk solid one. This is the standard, mostly used, approach to interpolate the interfacial FE density. It is obvious that this approach reaches its limit when one of the two phases does not exist in the whole concentration range of the interface. This is the case when dealing with growth kinetics for alloy systems in which the solid phase has a very small solubility or is even a stochiometric line phase. The approaches of Steinbach *et al.*[50] and Kim *et al.*[51] start from a more realistic representation of the interface. They consider the interface as a mixture of two phases with different compositions, which may be the respective equilibrium bulk compositions. They further impose that the chemical potential in both interface phases must be the same. This representation of the interface more closely reflects the picture gained from MD modeling, where the interface appears as the cohabitation of two phases related to their respective bulk regions. The concentration gradient at the interface results then from the variation in the fraction of each phase within the interface.

V. CONCLUSIONS

In this work, we address the question whether MD simulations and PF modeling give the same quantitative physical

description of the solidification and melting kinetics in a crystal-liquid structure of an alloy system under nonequilibrium conditions. Testing this equivalence is important as it gives an idea about the range of applicability of both approaches and allows to verify whether physical parameter can, without further ado, be exchanged between the two computational methods when trying to bridge the gap between atomistic and mesoscopic modeling. The nonequilibrium conditions are realized by subjecting a solid-liquid layered sample, equilibrated at temperature T, to an abrupt temperature change ΔT above or under the liquidus line, creating in this way a supersaturated or undersaturated solution, respectively. In this regard, the present computer experiments are different from most cases encountered in literature, which deal either with monatomic systems or intermetallic phases. The additional solute concentration effect considered in our study makes that the transformation kinetics does not only depend on the difference between the FE of the two phases but also on the difference between the chemical potentials (related to the derivative of the FE) of the individual species in the solution. This requires an additional care in constructing the concentration dependent FEs of the different phases. Our PF simulations of NiZr alloy use the FE density calculated within a thermodynamic MD-based approach. Usually, the methods used by PF modeling to construct the FE of the different phases are based on approximation approaches of the interatomic interaction, mostly the ideal and regular solution models.

MD and PF modeling results agree well regarding the solidification and melting rates as well as the respective concentration profiles. Our study illustrates clearly that the PF approach is able to describe the same aspects of physics than MD, when the key physical parameters are transferred from the latter method to the former one. In other words, we show that a thermodynamic consistent PF model can be applied down to the range of atomistic structure, without thermodynamic concepts loosing their relevance at the atomic level. At the same time, MD modeling seems to be capable to treat correctly relaxation dynamics driven by thermodynamics forces in a nonequilibrium state. Moreover, thermodynamic and kinetic properties such as the FE, the phase diagram, and the diffusivity-calculated for equilibrium conditions, turn out to be a sufficient approximation for describing nonequilibrium situations. It goes without saying that we cannot pretend to the generality of our conclusions as one has to prove their validity by considering other MD-based studies for different alloy systems. Moreover, our study points out that bridging the gap between PF and MD approaches offers potential to a better understanding of the thermodynamic and kinetic processes underlying the solidification and melting processes. On the one side, PF modeling offers the possibility for analyzing the separate contribution of the different physical parameters affecting the phase transformation processes, such as the FE density, the interface width ε, and the surface tension σ. In so doing, we are able to clearly demonstrate the dominant diffusive character of solidification and melting of a two-phase NiZr system out of chemical equilibrium, the interface properties σ and ε playing thereby a relatively secondary role. A sharp-interface analysis confirms this result. Comparison with the ideal solution model used in our earlier work[6] enables to quantify the weight of the thermodynamics of mixing in the growth process. On the other side, the MD approach, in addition to provide the necessary key parameters, may also provide a valuable support in designing and calibrating the rather phenomenological PF model. For instance, the picture gained from MD simulation about the atomic properties (morphology and dynamics) of and at the interface may constitute the basis to construct a FE function that better reflects these properties. Our study points out the shortcoming of the standard interpolation procedure to describe the FE of the interface when one of the phases cannot be defined over the whole concentration gradient of the interface. Moreover, the MD study reveals that the confinement effect caused by the crystalline wall at low temperature has to be included when constructing the phase-dependent diffusivity.[48] A deep understanding of the kinetic processes that take place on the atomic scale at the solid-liquid interface during crystallization in alloys is a prerequisite for elaborating a model for growth and melting in these materials. Such a model still is lacking until now.

ACKNOWLEDGMENTS

This work was supported by the German Research Foundation (DFG) under the research training group 1483. Abhik Choudhury is acknowledged for useful discussions.

*Present address: Karlsruher Institut für Technologie (KIT), Zoologisches Institut, Theoretische Biophysik.

[1] J. J. de Pablo and W. A. Curtin, MRS Bull. **32**, 905 (2007).
[2] W. E, B. Engquist, and Z. Huang, Phys. Rev. B **67**, 092101 (2003).
[3] A. Ramasubramaniam and E. A. Carter, MRS Bull. **32**, 913 (2007).
[4] J. J. Hoyt, M. Asta, and A. Karma, Mater. Sci. Eng. R. **41**, 121 (2003).
[5] J. Bragard, A. Karma, Y. Lee, and M. Plapp, Interface Sci. **10**, 121 (2002).
[6] D. Danilov, B. Nestler, M. Guerdane, and H. Teichler, J. Phys. D **42**, 015310 (2009).
[7] K.-B. Küchemann, Ph.D. thesis, University of Göttingen, 2004.
[8] H. Teichler and M. Guerdane, in *Phase Transformations in Multicomponent Melts*, edited by D. M. Herlach and R. Kirchheim (Wiley-VCH, Weinheim, 2008).
[9] H. Teichler, Phys. Rev. Lett. **76**, 62 (1996); A. B. Mutiara and H. Teichler, Phys. Rev. E **64**, 046133 (2001); I. Ladadwa and H. Teichler, *ibid.* **78**, 041503 (2008).
[10] A. Karma, *Encyclopedia of Materials Science and Technology* (Elsevier, Oxford, 2001).
[11] W. J. Boettinger, J. A. Warren, C. Beckermann, and A. Karma, Annu. Rev. Mater. Res. **32**, 163 (2002).

[12] J. J. Hoyt, M. Asta, and A. Karma, Phys. Rev. Lett. **86**, 5530 (2001).
[13] H. Teichler, Phys. Rev. B **59**, 8473 (1999).
[14] H. E. A. Huitema, M. J. Vlot, and J. P. van der Eerden, J. Chem. Phys. **111**, 4714 (1999).
[15] F. Celestini and J. M. Debierre, Phys. Rev. B **62**, 14006 (2000).
[16] H. A. Wilson, Philos. Mag. **50**, 238 (1900).
[17] J. Frenkel, Phys. Z. Sowjetunion **1**, 498 (1932).
[18] J. Q. Broughton, G. H. Gilmer, and K. A. Jackson, Phys. Rev. Lett. **49**, 1496 (1982).
[19] K. A. Jackson, Interface Sci. **10**, 159 (2002).
[20] J. J. Hoyt, M. Asta, and A. Karma, Interface Sci. **10**, 181 (2002).
[21] A. Kerrache, J. Horbach, and K. Binder, EPL **81**, 58001 (2008).
[22] K. R. Elder, M. Katakowski, M. Haataja, and M. Grant, Phys. Rev. Lett. **88**, 245701 (2002).
[23] K. A. Wu and A. Karma, Phys. Rev. B **76**, 184107 (2007).
[24] P. Y. Chan, N. Goldenfeld, and J. Dantzig, Phys. Rev. E **79**, 035701(R) (2009).
[25] Ch. Hausleitner and J. Hafner, Phys. Rev. B **45**, 115 (1992).
[26] Ch. Hausleitner and J. Hafner, Phys. Rev. B **45**, 128 (1992).
[27] *Binary Alloy Phase Diagrams*, edited by T. B. Massalski (ASM International, Metal Park, Ohio, 1990).
[28] Th. Voigtmann, A. Meyer, D. Holland-Moritz, S. Stüber, T. Hansen, and T. Unruh, EPL **82**, 66001 (2008).
[29] H. Teichler, Defect Diffus. Forum **143-147**, 717 (1997).
[30] H. Teichler, J. Non-Cryst. Solids **293-295**, 339 (2001).
[31] R. S. Averback, Mater. Res. Bull. **16**, 47 (1991).
[32] J. J. Hoyt, B. Sadigh, M. Asta, and S. M. Foiles, Acta Mater. **47**, 3181 (1999).
[33] A. Karma and W.-J. Rappel, Phys. Rev. E **57**, 4323 (1998).
[34] B. Stinner, B. Nestler, and H. Garcke, SIAM J. Appl. Math. **64**, 775 (2004).
[35] B. Nestler, H. Garcke, and B. Stinner, Phys. Rev. E **71**, 041609 (2005).
[36] F. Otto and W. E, J. Chem. Phys. **107**, 10177 (1997).
[37] M. Guerdane and H. Teichler, Phys. Rev. Lett. **101**, 065506 (2008).
[38] P. Haasen, *Physical Metallurgy* (Cambridge University Press, Cambridge, 1996).
[39] P. J. Steinhardt, D. R. Nelson, and M. Ronchetti, Phys. Rev. B **28**, 784 (1983).
[40] B. Vinet, L. Magnusson, H. Fredriksson, and P. J. Desre, J. Colloid Interface Sci. **255**, 363 (2002).
[41] B. Böddeker and H. Teichler, Phys. Rev. E **59**, 1948 (1999).
[42] G. Vogl, W. Miekeley, A. Heidemann, and W. Petry, Phys. Rev. Lett. **53**, 934 (1984); A. Heiming, W. Petry, J. Trampenau, W. Miekeley, and J. Cockcroft, J. Phys.: Condens. Matter **4**, 727 (1992).
[43] G. M. Hood and R. J. Schultz, Philos. Mag. **26**, 329 (1972).
[44] J. C. Barbour, F. W. Saris, M. Nastasi, and J. W. Mayer, Phys. Rev. B **32**, 1363 (1985).
[45] V. Witusiewicz and F. Sommer, Metall. Mater. Trans. B **31**, 277 (2000).
[46] N. Karpe, J. P. Krog, J. Bøttiger, N. G. Chechenin, R. E. Somekh, and A. L. Greer, Acta Metall. Mater. **43**, 551 (1995).
[47] M. Guerdane and H. Teichler, Phys. Rev. B **65**, 014203 (2001); M. Guerdane, Ph.D. thesis, Universität Göttingen, 2000.
[48] A study is in progress concerning how this ordering and reduced mobility at the interface is coupling to the kinetic of nucleation and growth of the solidification process.
[49] F. Celestini and J. M. Debierre, Phys. Rev. E **65**, 041605 (2002).
[50] I. Steinbach, F. Pezzola, B. Nestler, M. Seeelberg, R. Prieler, G. J. Schmitz, and J. L. L. Rezende, Physica D **94**, 135 (1996).
[51] S. G. Kim, W. T. Kim, and T. Suzuki, Phys. Rev. E **60**, 7186 (1999).